Journal of Molecular Structure 1273 (2023) 134252

Contents lists available at ScienceDirect

Journal of Molecular Structure

journal homepage: www.elsevier.com/locate/molstr

The effect of structure parameters and static electric field on the nonlinear optical properties of triple InGaAs/GaAs quantum well

M. Sayrac[a,b,*], E. Kaynar[a,b], F. Ungan[c]

[a] Department of Nanotechnology Engineering, Sivas Cumhuriyet University, Sivas, Turkey
[b] Nanophotonics Research and Application Center, Sivas Cumhuriyet University, Sivas, Turkey
[c] Department of Physics, Sivas Cumhuriyet University, Sivas, Turkey

ARTICLE INFO

Article history:
Received 27 June 2022
Revised 28 September 2022
Accepted 30 September 2022
Available online 1 October 2022

Keywords:
Low dimensional structures
Quantum wells
Semiconducting $In_xGa_{1-x}As/GaAs$
Numerical Simulations

ABSTRACT

Optical properties of $In_xGa_{1-x}As/GaAs$ triple QW are studied for different quantum well thicknesses and external electric fields. The effective mass approximation is used to calculate the band alignment of the structure. The finite difference method (FDM) is applied to solve the 1D- Schrödinger equation. Intersubband energies and the total optical absorption coefficients (TOACs) and total relative refractive index changes (RRICs) are numerically calculated under the applied external electric field. The structure parameters and applied electric field cause the separation of the energy levels and variation of the dipole moment matrix elements. These separations are responsible for the resonant peak shifts. It is shown that the varied structure parameters and external electric field cause red or blue shifts in the resonant peak position of TOAC and RRIC coefficients.

1. Introduction

Recent growth technologies have made it possible to produce different low-dimensional semiconductor quantum systems. The quantum-based semiconductors have found broad usage in the study and application of light-emitting or detecting devices (optoelectronic electronic devices) [1–5].

III-V semiconductor materials have been investigated because of their integration into semiconductor devices [6–8]. Optimization of the structure parameters and the applied external fields modify the intersubband transitions because of the large quantum confinement effect [9–13]. Nonlinear optical properties such as second harmonic generation (SHG) and third harmonic generation (THG) as well as the absorption coefficients and relative refractive index changes have attracted a lot of interest because it gives detailed information about the behavior of the structure under the applied structure parameters and the external fields.

The nonlinear optical properties in different asymmetric structure shapes have been studied such as single quantum wells (QWs) [14, 15], multiple QWs [16, 17], and semi-parabolic QWs [18–20]. The investigation of these structures by controlling the structure parameters and applying external fields adjusts the amplitude and the position of the nonlinear optical properties. Yuan et al. investigated the SHG in the asymmetric Gaussian potential [21]. SHG in the symmetric and asymmetric Gaussian potentials has been studied, and it found that the resonant SHG peak depends on the applied electric field and the structure parameters [22]. Liu et al. explored the impact of temperature, magnetic field, and hydrostatic pressure on the SHG coefficients [23].

The investigation of low dimensional structure is the main interest since they find possible applications in technological devices. The shape of the QW profile affects the physical properties of the systems. For this reason, theoretical and experimental research has been carried out to obtain linear and nonlinear properties of this structure at different structure parameters and the applied external fields [24–33]. Some of the main studies are as follows: the effect of the electric field on the nonlinear optical properties of QWs [34], the optical absorption in symmetric double parabolic QWs [35], total optical absorption coefficients with Rosen–Morse confinement potential [36], the effect of impurities and optical intensities on the linear and nonlinear absorption coefficients, the relative refractive index changes in low dimensional systems [37], and the optical absorption coefficients and the refractive index changes of the superlattice [38]. Moreover, the optical properties of quantum dots (QDs) [39, 40], the effect of ILF [41], the electric field [42], and hydrostatic pressure [43] have been investigated. Understanding the linear and nonlinear optical properties of the low dimensional systems is critical because these optical properties of the structure are strongly affected by the structure parameters and the applied external fields.

* Corresponding author.
E-mail address: muhammedsayrac@cumhuriyet.edu.tr (M. Sayrac).

https://doi.org/10.1016/j.molstruc.2022.134252
0022-2860/

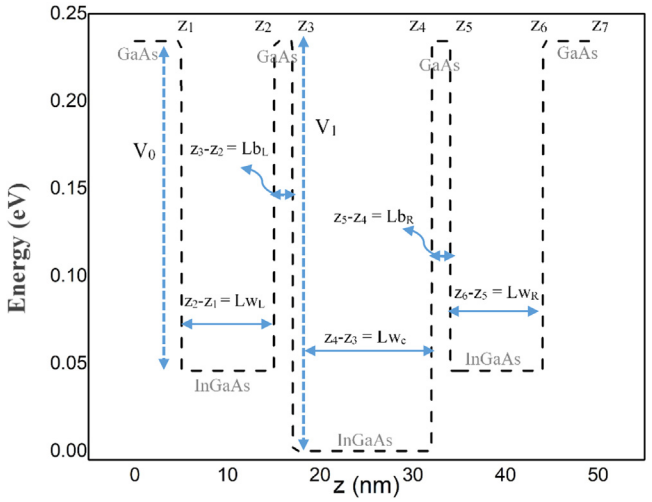

Fig. 1. Schematic representation of the triple GaAs/InGaAs quantum well. The index of structure parameters are as follows: z_2-z_1 = Lw_L for left QW width, z_3-z_2 = Lb_L for left barrier thickness, z_4-z_3 = Lw_c for center QW width, z_5-z_4 = Lb_R for right barrier thickness, z_6-z_5 = Lw_R for right QW width.

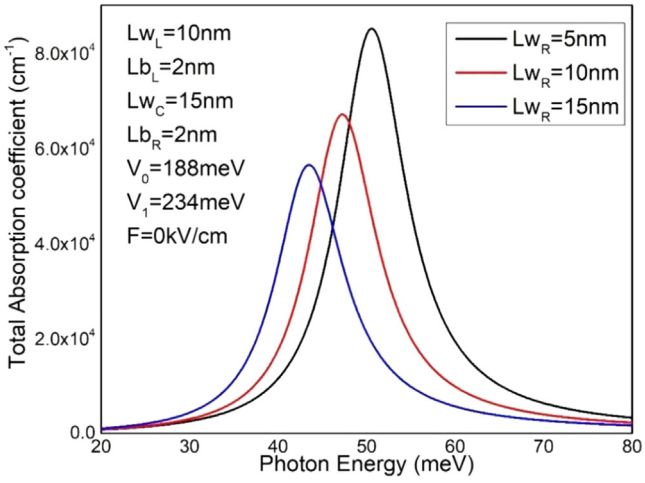

Fig. 3. Variation of total optical absorption coefficients as a function of incident photon energy for different values of Lw_R.

In this paper, the nonlinear optical properties such as the total optical absorption coefficients and relative refractive index changes of InGaAs/GaAs triple QW were investigated. The effect of structure parameters and applied external electric fields on these optical properties is discussed in detail. To perform the numerical simulations, firstly, the time-independent Schrödinger equation is numerically solved to obtain the subband energy values and their electronic wave functions of an electron confined in the conduction band of the structure. After that, using these electronic states obtained about the structure, the total optical absorption coefficients and relative refractive index changes of the system are calculated by using the compact-density matrix approach and iterative method. The organization of the paper is that Section 2 gives the theoretical background of the numerical calculations. Section 3 discusses the simulation result and compares the obtained results. Finally, a conclusion of the physical results obtained in the paper is given in Section 4.

2. Theoretical background

In this study, the effects of static electric field and structure parameters on the nonlinear optical properties of the InGaAs/GaAs triple quantum well, whose schematic representation is given in Fig. 1, are theoretically investigated. The static electric field along the z direction is applied to the structure. The quantum well structure with different confining potentials is investigated by controlling the structure parameters. The total Hamiltonian of an electron in this structure under the external applied electric field is given by [41, 44, 45]

$$H = \frac{\vec{p}_e^2}{2m^*} + V(z) - eF\vec{z} \tag{1}$$

where m^* is the electron effective mass, P_e is the electron momentum, F is the magnitude of the applied external electric field, and the z-axis is the growth direction of the structure.

The confinement potential $(V(z))$ for the electron in the z-direction is given by

$$V(z) = \begin{cases} V_0 & 0 < z < z_1 \\ (V_1 - V_0) & z_1 < z < z_2 \\ V_0 & z_2 < z < z_3 \\ 0 & z_3 < z < z_4 \\ V_0 & z_4 < z < z_5 \\ (V_1 - V_0) & z_5 < z < z_6 \\ V_0 & z_6 < z < z_7 \end{cases} \tag{2}$$

where V_0 and V_1 are the potential depths between GaAs/$In_xGa_{1-x}As$ for x=*0.2* and *0.25 in* concentration.

The solution of Eq. 1 under different structure parameters and external fields produces the variation of the subband energy states and the corresponding wave functions by using the diagonalization method [46]. In this method, the calculation of the single-electron wave function $\psi(z)$ is performed for infinite quantum well width L_∞, which is large compared to the triple QW widths. The wave

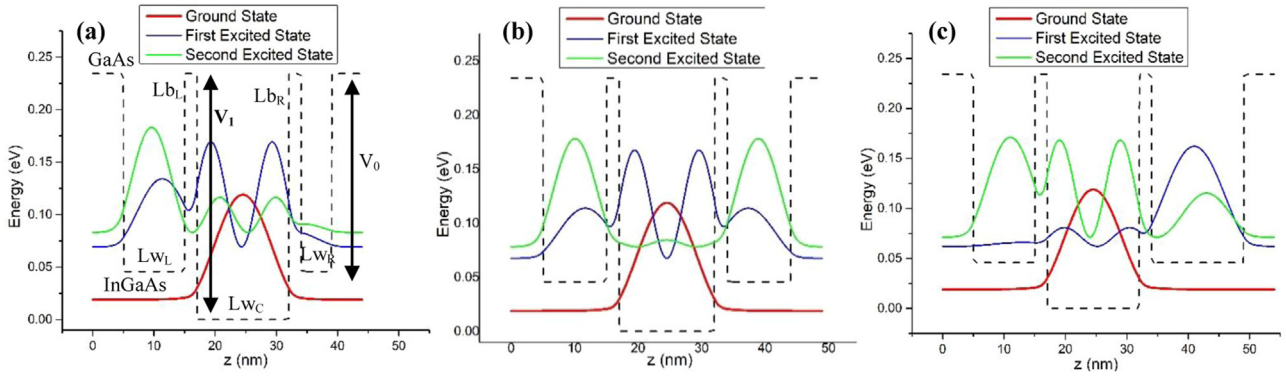

Fig. 2. Confining potential and first three excited state wavefunctions and corresponding energy levels at different Lw_R.

Table 1
The variation of the subband energy difference and dipole moment matrix elements for different Lw_R values.

Lw_R (nm)	E_{10} (meV)	μ_{00} (nm)	μ_{11} (nm)	μ_{10} (nm)
5	50.3393	24.5023	20.3460	3.3451
10	47.0126	24.5250	24.5233	3.0711
15	43.2408	24.5304	27.8556	2.9375

Table 2
The variation of the energy difference and dipole moment matrix elements for different Lb_R values.

Lb_R (nm)	E_{10} (meV)	μ_{00} (nm)	μ_{11} (nm)	μ_{10} (nm)
2	48.7126	24.5250	24.5233	3.3711
5	50.2489	24.4072	19.2335	3.170
7	52.3601	24.4037	18.8294	3.0593

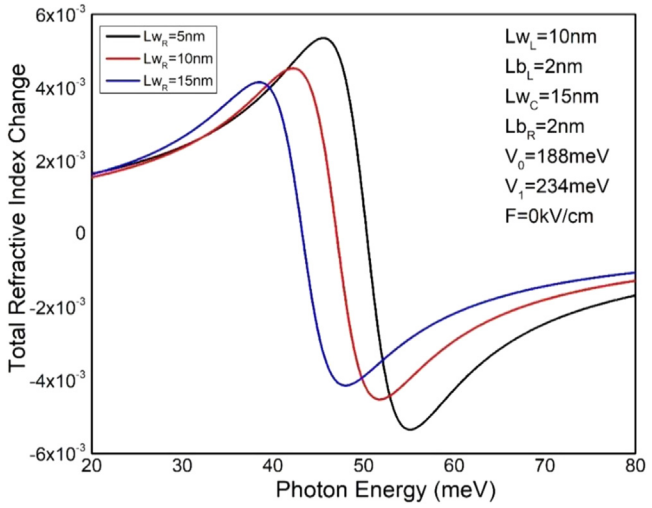

Fig. 4. Change in the relative refractive index changes as a function of the incident photon energy for three different Lw_R.

function describing the structure consists of the complete set is given

$$\psi(z) = \sqrt{\frac{2}{L_\infty}} \sum_{m=1}^{\infty} C_m \sin(m\pi \left[\frac{z}{L_\infty} + \frac{1}{2}\right]) \tag{3}$$

where C_m is the coefficients. After the energies and their corresponding wave functions are obtained, the linear, third-order nonlinear, total optical absorption coefficients (TOACs), and relative refractive index changes (RRICs) for transition for the electron states are analytically expressed under the compact density matrix approach and iterative method.

The system is excited by an electromagnetic field ω

$$E(t) = E_0 e^{i\omega t} + E_0 e^{-i\omega t} \tag{4}$$

The time evolution of one electron density operator ρ is written [47, 48]

$$\frac{\partial \rho}{\partial t} = \frac{1}{i\hbar}[H_0 - qxE(t), \rho] - \Gamma(\rho - \rho^{(0)}) \tag{5}$$

where H_0 is the Hamiltonian for the system without the electromagnetic field ($E(t)$), and q is the electron charge. $\rho^{(0)}$ is the unperturbed density matrix operator and $\Gamma$is responsible for the electron-phonon interaction and collisions among electrons. Γ is a diagonal matrix element that equals the inverse of relaxation time T. Equation 5 is solved by using the iterative approach [49]

$\rho(t) = \sum_n \rho^{(n)}(t)$,

with (6)

$$\frac{\partial \rho_{ij}^{(n+1)}}{\partial t} = \frac{1}{i\hbar}[H_0, \rho^{(n+1)}] - \Gamma_{ij}\rho_{ij}^{(n+1)} - \frac{1}{i\hbar}[qx, \rho^{(n)}]_{ij}E(t)$$

To simplify the analytical solution, we consider two-level electronic systems for electronic transitions. The electronic polarization $P(t)$ and susceptibility $\chi(t)$ are given by dipole operator M_{ij} and density matrixρ:

$$P(t) = \varepsilon_0 \chi(\omega) E_0 e^{-i\omega t} + \varepsilon_0 \chi(-\omega) E_0^* e^{i\omega t} = \frac{1}{V} Tr(\rho M) \tag{7}$$

where ε_0 is the permittivity of free space and Tr (trace) means the summation over the diagonal matrix elements. The analytical forms of the linear$\chi^{(1)}$and the third-order nonlinear$\chi^{(3)}$susceptibility coefficients are obtained from Eqs. 6, 7.

The absorption coefficient and refractive index changes are related to susceptibility [50].

$$\beta(\omega) = \omega \sqrt{\frac{\mu}{\varepsilon_R}} \mathrm{Im}[\varepsilon_0 \chi(\omega)] \tag{8}$$

$$\frac{\Delta n(\omega)}{n_r} = \mathrm{Re}\left[\frac{\chi(\omega)}{2n_r^2}\right] \tag{9}$$

Now we can give the analytical formula for the linear and third-order nonlinear absorption coefficients and relative refractive index changes. These expressions are defined as follows [42, 51]

$$\beta^{(1)}(\omega) = \omega \sqrt{\frac{\mu}{\varepsilon_r}} \frac{|M_{10}|^2 \sigma_v \hbar \Gamma_{10}}{(E_{10} - \hbar\omega)^2 + (\hbar\Gamma_{10})^2} \tag{10}$$

$$\frac{\Delta n^{(1)}(\omega)}{n_r} = \frac{\sigma_v |M_{10}|^2}{2n_r^2 \varepsilon_0} \left[\frac{E_{10} - \hbar\omega}{(E_{10} - \hbar\omega)^2 + (\hbar\Gamma_{10})^2}\right] \tag{11}$$

$$\beta^{(3)}(\omega, I) = -2\omega \sqrt{\frac{\mu}{\varepsilon_r}} \left(\frac{I}{\varepsilon_0 n_r c}\right) \frac{|M_{10}|^4 \sigma_v \hbar \Gamma_{10}}{\left[(E_{10} - \hbar\omega)^2 + (\hbar\Gamma_{10})^2\right]^2}$$
$$\left[1 - \frac{|M_{11} - M_{00}|^2}{|2M_{10}|^2} \times \frac{(E_{10} - \hbar\omega)^2 - (\hbar\Gamma_{10})^2 + 2(E_{10})(E_{10} - \hbar\omega)}{(E_{10})^2 + (\hbar\Gamma_{10})^2}\right]. \tag{12}$$

$$\frac{\Delta n^{(3)}(\omega, I)}{n_r} = -\frac{\mu c |M_{10}|^2}{4n_r^3 \varepsilon_0} \frac{\sigma_v I}{\left[(E_{10} - \hbar\omega)^2 + (\hbar\Gamma_{10})^2\right]^2} \times \left[4(E_{10} - \hbar\omega)|M_{10}|^2\right]$$
$$\left[-\frac{(M_{11} - M_{00})^2}{(E_{10})^2 + (\hbar\Gamma_{10})^2} \left\{(E_{10} - \hbar\omega) \times \left[(E_{10})(E_{10} - \hbar\omega) - (\hbar\Gamma_{10})^2\right]\right.\right.$$
$$\left.\left. - (\hbar\Gamma_{10})^2 (2(E_{10}) - \hbar\omega)\right\}\right] \tag{13}$$

where ω presents the angular frequency and Γ is relaxation time for intersubband transitions. μ and ε_r are magnetic permeability and the real part of the electrical permittivity. σ_v is the carrier density, $\hbar$ is the Planck constant and n_r is the refractive index. E_{ij} is the i^{th} and j^{th} energy state of the electron. M_{ij} corresponds to transition dipole element.

The total TOACs and RRICs equal the sum of the linear and third-order nonlinear terms and are given by the following equation:

$$\beta(\omega, I) = \beta^{(1)}(\omega) + \beta^{(3)}(\omega, I) \tag{14}$$

and

$$\frac{\Delta n(\omega, I)}{n_r} = \frac{\Delta n^{(1)}(\omega)}{n_r} + \frac{\Delta n^{(3)}(\omega, I)}{n_r} \tag{15}$$

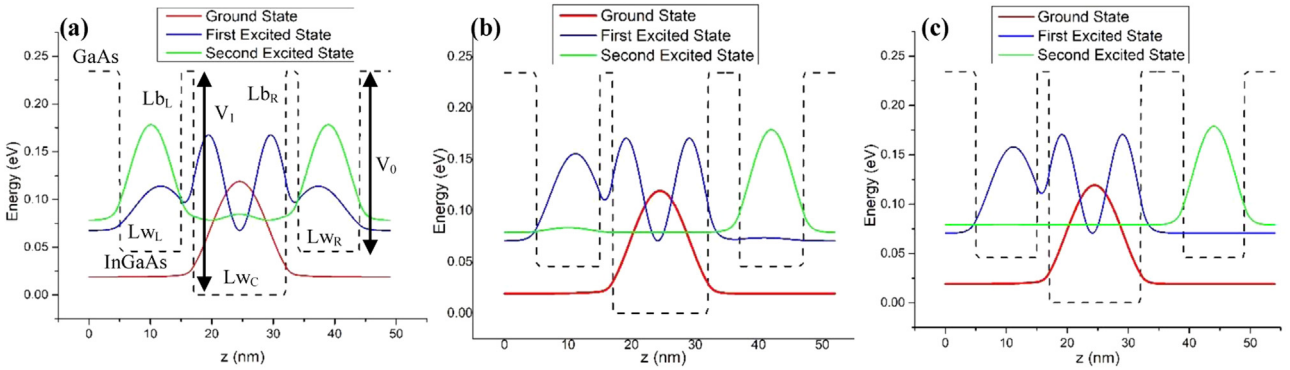

Fig. 5. Confining potential and first three excited state wavefunctions and corresponding energy levels at different Lb_R.

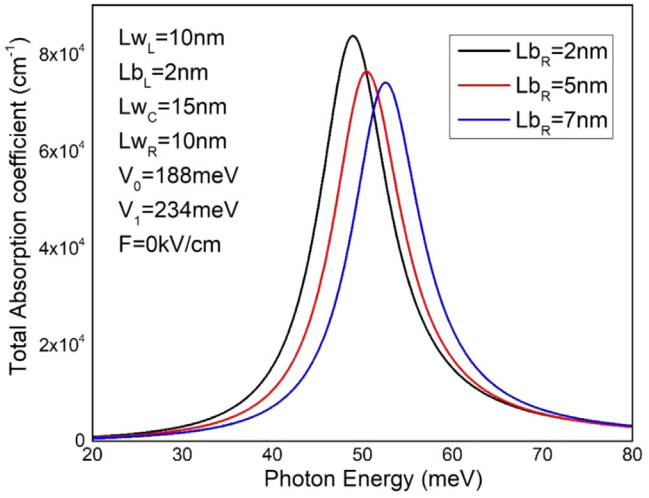

Fig. 6. The total optical absorption coefficients as a function of incident photon energy at different Lb_R values.

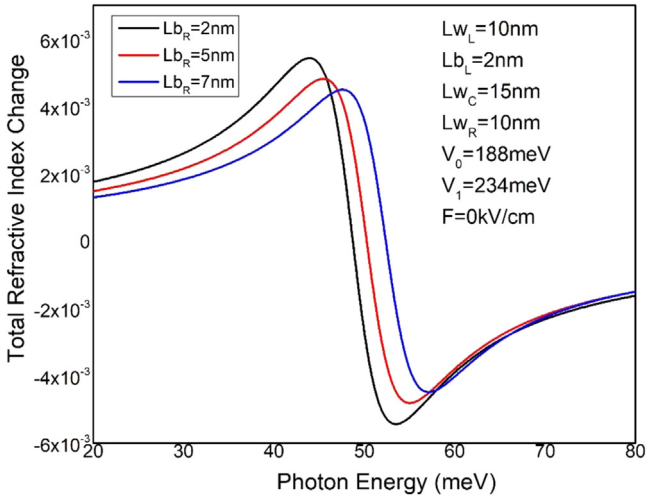

Fig. 7. The relative refractive index changes for three different Lb_R values.

where the relative refractive index of the system is $n_r = \sqrt{\varepsilon_r}$ and the real part of the permittivity is $\varepsilon_R = n_r^2 \varepsilon_0$. ε_0 and μ_0 are vacuum permittivity and vacuum permeability, respectively. σ_υ is the carrier density of the system. ω is the angular frequency of the incident photon, I is the optical intensity of the incident photon, E_{10} is the energy difference between the two lowest energy levels and Γ_{10} is defined as the relaxation rate for states 1 and 0. $M_{ij} = \langle \psi_i(z)|ez|\psi_j(z)\rangle$ (here $i,\ j = 0,\ 1$) represents the dipole moment matrix element for the transitions.

3. Result and discussion

The physical values of simulation input parameters are listed as [52–55]: $m^* = 0.059m_0$ (m_0 is the free electron mass), $c = 3 \times 10^8 m/s$, $e = 1.602 \times 10^{-19}$ C, $\hbar = 1.056 \times 10^{-34}$Js, $\sigma_\nu = 3 \times 10^{22} m^{-3}$, $\mu = 4\pi \times 10^7 Hm^{-1}$, $\varepsilon = 12.58$, $\varepsilon_0 = 8.854 \times 10^{-12}$, $I = 0.01 \frac{MW}{cm^2}$, $\tau_{12} = 0.14$ ps and $n_r = 3.9$. Discontinuity of conduction band of $In_xGa_{1-x}As/GaAs$ is given as V_0^{InGaAs}=*%60*(E_g^{GaAs}-E_g^{InGaAs}) [56], where E_g^{InGaAs}=*(E_g^{GaAs}-1619x-555x²)*meV and E_g^{GaAs}=*1424meV*. Therefore, the potential depths for the center well (V_1) and side wells (V_0) are 234meV (*x=0.25*) and 188meV (*x=0.20*), respectively. We first examine the structure parameters' effects and the applied

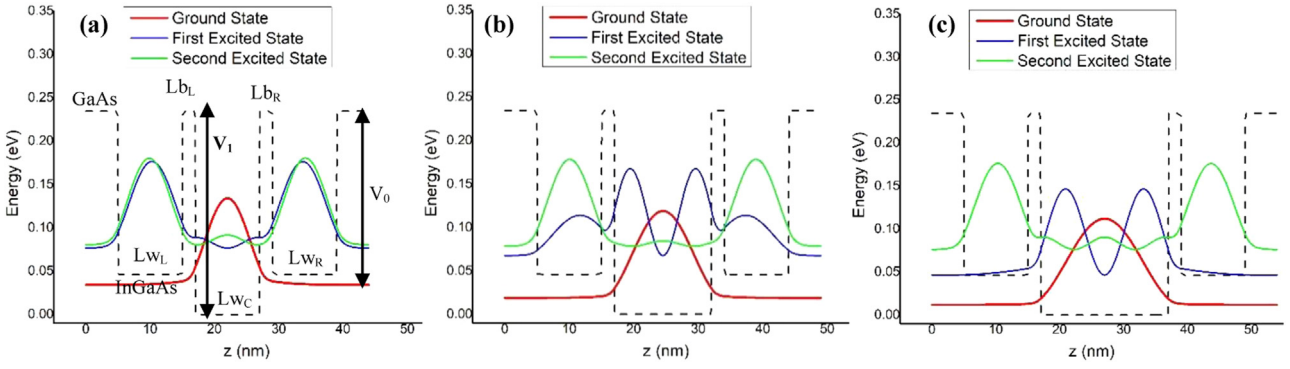

Fig. 8. Shape of InGaAs/GaAs potential structure for different Lw_c values and corresponding wavefunctions and energy levels.

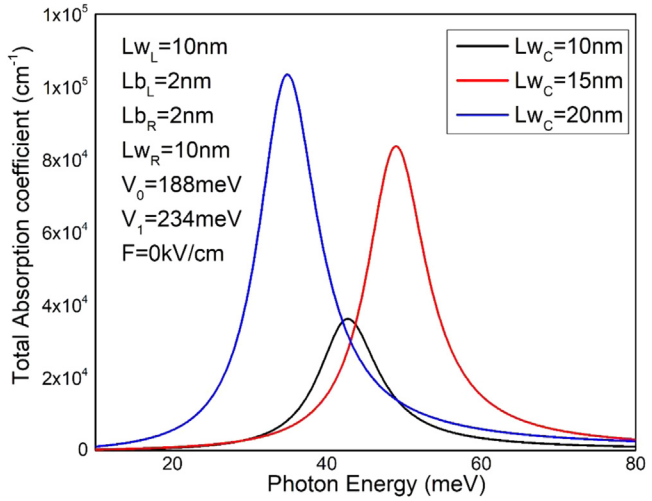

Fig. 9. Total absorption coefficients as a function of incident photon energy at three different Lw_c values.

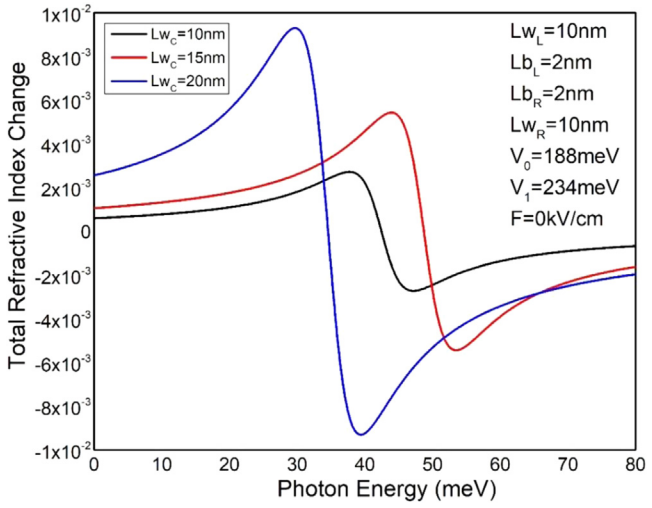

Fig. 10. The relative refractive index changes for three different center quantum well width values.

Table 3
The variation of the energy difference and dipole moment matrix elements for different Lw_c values.

Lw_c (nm)	E_{10} (meV)	μ_{00} (nm)	μ_{11} (nm)	μ_{10} (nm)
10	42.4407	22.0250	22.0126	2.3734
15	48.7126	24.5250	24.5233	3.3711
20	34.5556	27.025	27.025	4.4428

electric field on the energy level and the dipole moment matrix elements of the structure. Then, the effects of the external field and the structural parameters on total optical absorption coefficients (TOACs) and the relative refractive index changes (RRIC) of the system were investigated. The simulation is performed in two steps. The first step is that the single parabolic band and effective mass approaches are applied to obtain energy eigenvalues and eigenfunctions of the electron. In the second step, TOACs and RRICs for transition for the electron states are analytically expressed under the compact density matrix approach and iterative method. The applied static electric field results in the red/blue shifts of the TOACs and RRIC peak position. The applied external field brings additional freedom to control the physical properties of the system. The effects of the structure parameters and the applied external

Table 4
The variation of the energy difference and dipole moment matrix elements for different applied external electric fields.

F kV/cm	E_{10} (meV)	μ_{00} (nm)	μ_{11} (nm)	μ_{10} (nm)
0	48.7126	24.5250	24.5233	3.3711
60	46.2567	24.2095	22.4747	2.9419
120	40.3311	23.8842	22.5546	2.4356

electric field on the TOACs and RRIC of the InGaAs/GaAs QW structure are detailed and investigated in each subsection below.

3.1. Effect of right-well width (Lw_R)

The triple QW is conceptualized by inserting the InGaAs QW surrounded by GaAs barriers, Fig.Fig. 2. The structure is subjected to variation of the right QW width (Lw_R) for 5nm, 10nm, and 15nm. The structure parameters (except Lw_R) are kept constant as well as the applied electric field: the left well width (Lw_L=10nm), the left barrier thickness (Lb_L=2nm), the center well width (Lw_c=15nm), and right barrier thickness (Lb_R=2nm). The potential depths are $V_0 = 188$ meV for the left and right QW and $V_1 = 234$ meV for the center QW. In addition, there are no applied external fields on the structure ($F = 0$). The shape of the potential profile is controlled by considering the above parameters. The variation of Lw_R results in the change of the ground state and excited state wavefunctions. The ground state wavefunction is confined in the deepest InGaAs QW. However, the first and second excited wavefunction is mostly confined in InGaAs well and with penetration in GaAs barrier.

Table 1 gives the energy difference between the ground state and the first excited state energy difference (E_{10}) as well as the dipole moment matrix elements. By using the simulated values presented in Table 1, the TOACs as a function of the incident photon energy for three values of the Lw_R are numerically calculated, Fig.Fig. 3. The amplitude of the TOACs decreases with Lw_R, and the peak position of that moves towards the lower energies (red-shift). The physical explanation of this trend is that dipole moment matrix elements (M_{10}) decrease with the increment of the Lw_R, and so the ground and first excited state energy difference decreases.

Fig.Fig. 4 displays the change in the RRICs for three different Lw_R values. The changes in the RRICs trend to redshifts. Furthermore, the amplitude of the change in RRICs decreases with the variation of Lw_R. These trends arise since the energy separation (E_{10}) decreases and results in the red-shift of the RRIC peak position and the dipole moment matrix element (M_{10}) decreases with the increment of Lw_R.

3.2. Effect of right barrier thickness (Lb_R)

In this section, we propose a structure composed of triple QWs for different right barrier thicknesses (Lb_R). The TOACs and RRICs are examined as a function of the incident photon energy, Fig.Fig. 5. The variation of Lb_R causes the variation of the ground state and excited state wavefunctions. Effects of the right barrier thickness (Lb_R) on the wave function and energy eigenvalues of the structure are investigated. Lb_R is set to 2 nm, 5 nm, and 7 nm, respectively. The constant structure parameters are as follows: the left well width ($Lw_L = 10$nm), the left barrier thickness ($Lb_L = 2$nm), the center well width ($Lw_c = 15$nm), and the right QW width ($Lw_R = 10$nm). The left and right QW depths are $V_0 = 188$meV and the center QW depth is $V_1 = 234$meV. In addition, there are no applied external fields on the structure (F=0). The shape of the QW structure is monitored by considering the above parameters.

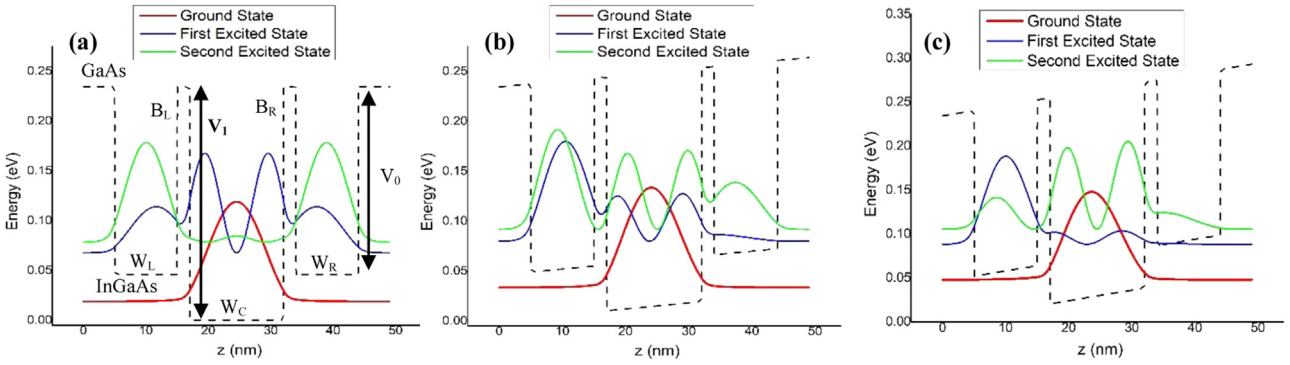

Fig. 11. InGaAs/GaAs potential shape for applied external electric fields and corresponding wavefunctions.

Table 2 exhibits the ground and first excited state energy difference and the dipole moment matrix elements. These parameters have direct control of the amplitude and the peak position of the TOACs and RRICs.

The numerical values in Table 2, TOAC as a function of the incident photon energy for different right barrier thickness values are numerically obtained in Fig. 6. The amplitude of TOAC gradually decreases while the peak position of that shifts to higher energy values (blue-shift). The control of the TOAC for different Lb_R values is due to the ground and first excited states' energy difference increasing with the increment of Lb_R. The dipole moment matrix elements decrease so the amplitude of TOAC decreases.

Fig. 7 exhibits RRIC for three different Lb_R values. The peak position of the refractive indices trends the blue shifts. Furthermore, the amplitude of the RRIC decreases with the variation of Lb_R. These trends arise since the energy separation between the ground state and the first excited state increases and results in the blue shift of the RRIC peak position. The amplitude of the RRIC is governed by the dipole moment matrix elements which decrease with the increment of Lb_R.

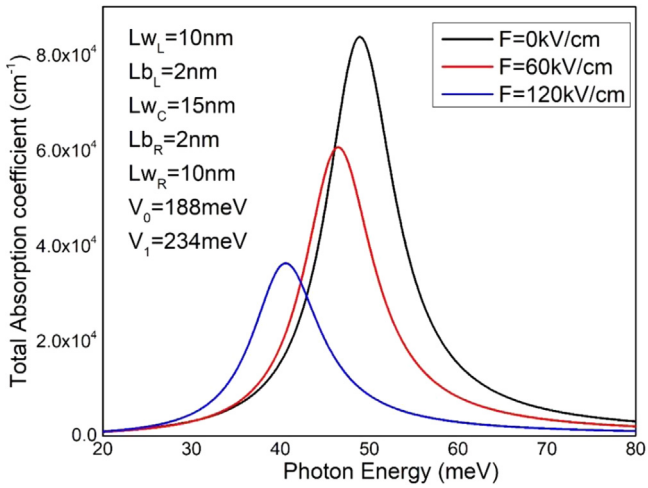

Fig. 12. Total optical absorption coefficients as a function of incident photon energy at three different applied electric fields.

3.3. Effect of center barrier width (Lw_c)

In this part, we examine GaAs/InGaAs structure for different triple QWs for different center QW widths (Lw_c). The nonlinear optical coefficients as a function of incident photon energy are investigated for different Lw_c values, Fig. 8. The center barrier width (Lw_c) is changed from 10nm to 20nm with a step of 5nm while the other parameters are kept constant; the left well width (Lw_L=10nm), the left and right barrier thickness (Lb_L=2nm, Lb_R=2nm), and the right QW width (Lw_R=10nm). The left and right QW depths are set to V_0=188meV, and the center QW depth is V_1=234meV. In addition, there are no applied external fields on the structure (F=0kV/cm). The shape of the potential profile is only controlled by considering the center barrier width (Lw_c).

Table 3 presents the calculated values of energy difference and dipole moment matrix elements. These values numerically depict the TOAC coefficients as a function of incident photon energy, Fig. 9. The ground and first excited state energy difference increases when the Lw_c increase from 10 nm to 15 nm. Then, the increment of Lw_c to 20 nm brings a noticeable decrease in the energy difference. These energy difference variations cause the initial blueshift and then cause the redshift to the peak position. The amplitude of the TOAC coefficient is controlled by the variation of the dipole moment matrix elements, which increases with the increment of the center quantum barrier width.

Fig. 10 exhibits RRIC for three different Lw_c values. The resonant peak position of the refractive indices initially shifts the higher energy (blue shift) and shifts the lower energy (red shift). This effect is due to variation of the ground state and first excited state energy difference, Table 3. In addition, the amplitude of the RRIC increases with the variation of the quantum well width of Lw_c. RRIC yield is controlled by the dipole moment matrix elements.

3.4. Effect of applied external electric field (F)

After examining the effects of the structure parameters on the TOAC and RRIC coefficients, the applied electric field (F) on the GaAs/InGaAs QW structure is examined. In this part, we investigated the effects of the applied external electric field on the structure profile. The F field is adjusted to 0, 60, and 120 kV/cm. The QW potential parameters are set as: the left well width (Lw_L=10nm), the left and right barrier thickness (Lb_L=2nm, Lb_R=2nm), the center QW width (Lw_c=15nm), and the right QW width (Lw_R=10nm). The left and right QW depths are V_0=188meV and the center QW depth is V_1=234meV. The applied electric field tilts the QW potential, i.e. electron feels tilted QW structure, and they occupy different energy levels and different wavefunctions, Fig. 11. The TOACs and RRICs are investigated at three different applied electric field values.

The obtained numerical values for the energy difference and the dipole moment matrix elements for different external electric fields are given in Table 4. By using these numerical values, TOACs are presented for different F values, Fig. 12. The increment of F values results in the decrease of the energy difference values. This energy variation causes the redshift of the TOAC peak, Fig. 12. The dipole moment matrix elements decrease with the applied exter-

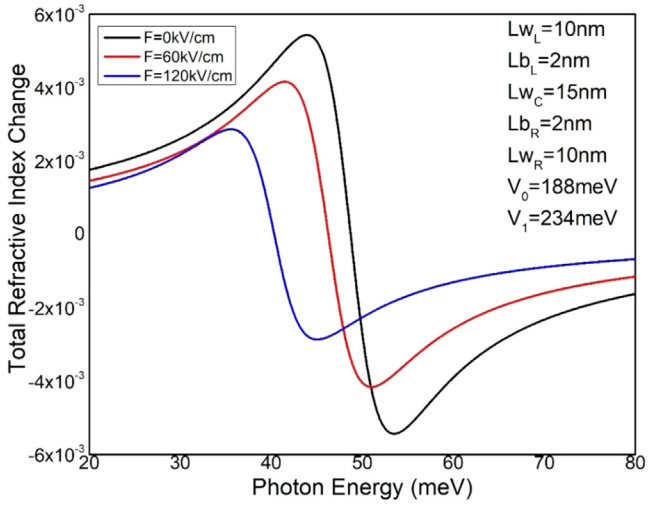

Fig. 13. The relative refractive index changes at different applied external fields.

nal electric field, and these variations cause the amplitude drop of the TOAC peak.

Fig. 13 presents the RRICs as a function of the incident photon energy. The RRIC peak position shifts to a lower energy region (redshift) with the applied external electric field since the energy difference decreases with the increment of the external field. The amplitude of the RRIC peaks is governed by the dipole moment matrix elements, which decrease with the applied external electric field.

4. Conclusion

In general, the total optical absorption coefficient and relative refractive index changes of the $In_xGa_{1-x}As/GaAs$ triple quantum well, which is favorable for the design and fabrication of new photodetectors, have been extensively studied under the influence of structure parameters and applied electric field. The variation of these parameters gives us additional freedom to monitor the peak position and peak amplitude of TOACs and RRICs of the structure. The obtained numerical results show that the optical absorption coefficients and refractive index changes of the structure can be shifted to higher or lower energy regions by controlling the structure parameters and external fields. These numerical simulations and analyzes have shown that these materials have the potential to develop new photodetectors and optoelectronic devices that operate especially in the infrared and far-infrared regions of the electromagnetic spectrum.

Declaration of Competing Interest

The authors declare that they have no known competing financial interests or personal relationships that could have appeared to influence the work reported in this paper.

CRediT authorship contribution statement

M. Sayrac: Software, Writing – original draft, Formal analysis. **E. Kaynar:** Writing – review & editing, Validation, Visualization. **F. Ungan:** Validation, Supervision, Writing – review & editing, Writing – original draft.

Data Availability

Data will be made available on request.

References

[1] J. De Jesus, G. Chen, L.C. Hernandez-Mainet, A. Shen, M.C. Tamargo, Strain compensated CdSe/ZnSe/ZnCdMgSe quantum wells as building blocks for near to mid-IR intersubband devices, J. Cryst. Growth 425 (2015) 207–211.
[2] I. Saidi, M. Gassoumi, H. Maaref, H. Mejri, C. Gaquière, Self-heating and trapping effects in AlGaN/GaN heterojunction field-effect transistors, J. Appl. Phys. 106 (2009) 054511.
[3] S.I. Gozu, T. Mozume, H. Kuwatsuka, H. Ishikawa, InGaAs/AlAs/InAlAs coupled double quantum wells for intersubband transition devices operating at 1550 nm, J. Cryst. Growth 378 (2013) 134–136.
[4] J. Feng, R. Akimoto, S.I. Gozu, T. Mozume, T. Hasama, H. Ishikawa, Band edge tailoring of InGaAs/AlAsSb coupled double quantum wells for a monolithically integrated all-optical switch, Opt. Express 21 (2013) 15840–15846.
[5] M. Sayrac, A. Turkoglu, M.E. Mora-Ramos, F. Ungan, Intensity-dependent nonlinear optical properties in an asymmetric Gaussian potential quantum well–modulated by external fields, Opt. Quantum Electron. 53 (2021) 485.
[6] J.C. Martínez-Orozco, I. Rodríguez-Vargas, C.A. Duque, M.E. Mora-Ramos, L.M. Gaggero-Sager, Study of the electronic properties of GaAs-based atomic layer doped field effect transistor (ALD-FET) under the influence of hydrostatic pressure, Phys. Status Solidi. B Basic Solid State Phys. 246 (2009) 581–585.
[7] J.G. Rojas-Briseño, J.C. Martínez-Orozco, I. Rodríguez-Vargas, M.E. Mora-Ramos, C.A. Duque, Nonlinear optical properties in an asymmetric double δ-doped quantum well with a Schottky barrier: electric field effects, Phys. Status Solidi. B Basic Solid State Phys. 251 (2014) 415–422.
[8] M. Sayrac, A. Turkoglu, F. Ungan, Influence of hydrostatic pressure, temperature, and terahertz laser field on the electron-related optical responses in an asymmetric double quantum well, Eur. Phys. J. B 94 (2021) 121.
[9] İ. Karabulut, H. Şafak, M. Tomak, Nonlinear optical rectification in asymmetrical semiparabolic quantum wells, Solid State Commun. 135 (2005) 735–738.
[10] L. Zhang, Electric field effect on the linear and nonlinear intersubband refractive index changes in asymmetrical semiparabolic and symmetrical parabolic quantum wells, Superlattices Microstruct. 37 (2005) 261–272.
[11] M.J. Karimi, A. Keshavarz, A. Poostforush, Linear and nonlinear intersubband optical absorption and refractive index changes of asymmetric double semi–parabolic quantum wells, Superlattices Microstruct. 49 (2011) 441–452.
[12] E. Ozturk, Depending on the electric and magnetic field of the linear optical absorption and rectification coefficient in triple quantum well, Opt. Quantum Electron. (2017) 49.
[13] M. Sayrac, Effects of applied external fields on the nonlinear optical rectification, second, and third-harmonic generation in an asymmetrical semi exponential quantum well, Opt. Quantum Electron. 54 (2021) 52.
[14] A. Liu, S.L. Chuang, C.Z. Ning, Piezoelectric field-enhanced second-order nonlinear optical susceptibilities in wurtzite GaN/AlGaN quantum wells, Appl. Phys. Lett. 76 (2000) 333–335.
[15] I. Saidi, Single- and double-resonant enhancement of second-harmonic generation in asymmetric AlGaN/GaN/AlGaN quantum well heterostructures, J. Appl. Phys. 125 (2019) 185702.
[16] A. Rostami, H. Baghban Asghari Nejad, H.Rasooli Saghai, Highly enhanced second-order nonlinear susceptibilities in tailored GaN–AlGaN–AlN quantum well structures, Physica B 403 (2008) 2725–2731.
[17] F. Wu, W. Tian, J. Zhang, S. Wang, Q.X. Wan, J.N. Dai, Z.H. Wu, J.T. Xu, X.Y. Li, Y.Y. Fang, C.Q. Chen, Double-resonance enhanced intersubband second-order nonlinear optical susceptibilities in GaN/AlGaN step quantum wells, Opt. Express 22 (2014) 14212–14220.
[18] J.-H. Yuan, Y. Zhang, H. Mo, N. Chen, Z. Zhang, The second-harmonic generation susceptibility in semiparabolic quantum wells with applied electric field, Optics Commun. 356 (2015) 405–410.
[19] H. Hassanabadi, G. Liu, L. Lu, Nonlinear optical rectification and the second-harmonic generation in semi-parabolic and semi-inverse squared quantum wells, Solid State Commun. 152 (2012) 1761–1766.
[20] I. Saidi, L. Bouzaïene, H. Maaref, H. Mejri, Optical nonlinearities in delta-doped AlGaN/GaN quantum well heterostructures, J. Appl. Phys. 101 (2007) 094506.
[21] Y. Jian-Hui, Z. Zhi-hai, Superlattice. Microst. 88 (2015) 1.
[22] J.-H. Yuan, N. Chen, H. Mo, Y. Zhang, Z.-H. Zhang, The second harmonic generation in symmetrical and asymmetrical Gaussian potential quantum wells with applied electric field, Superlattices Microstruct. 88 (2015) 389–395.
[23] X. Liu, L. Zou, C. Liu, Z.-H. Zhang, J.-H. Yuan, The nonlinear optical rectification and second harmonic generation in asymmetrical Gaussian potential quantum well: effects of hydrostatic pressure, temperature and magnetic field, Opt. Mater. 53 (2016) 218–223.
[24] L. Lu, W. Xie, Z. Shu, Combined effects of hydrostatic pressure and temperature on nonlinear properties of an exciton in a spherical quantum dot under the applied electric field, Physica B 406 (2011) 3735–3740.
[25] E. Ozturk, I. Sokmen, Nonlinear intersubband absorption and refractive index changes in square and graded quantum well modulated by temperature and Hydrostatic pressure, J. Lumin. 134 (2013) 42–48.
[26] M. Kirak, Y. Altinok, S. Yilmaz, The effects of the hydrostatic pressure and temperature on binding energy and optical properties of a donor impurity in a spherical quantum dot under external electric field, J. Lumin. 136 (2013) 415–421.
[27] I. Karabulut, M.E. Mora-Ramos, C.A. Duque, Nonlinear optical rectification and optical absorption in GaAs–Ga1–xAlxAs asymmetric double quantum wells: combined effects of applied electric and magnetic fields and hydrostatic pressure, J. Lumin. 131 (2011) 1502–1509.

[28] J.C. Martínez-Orozco, M.E. Mora-Ramos, C.A. Duque, Nonlinear optical rectification and second and third harmonic generation in GaAs δ-FET systems under hydrostatic pressure, J. Lumin. 132 (2012) 449–456.
[29] G. Rezaei, S.Shojaeian Kish, Linear and nonlinear optical properties of a hydrogenic impurity confined in a two-dimensional quantum dot: effects of hydrostatic pressure, external electric and magnetic fields, Superlattices Microstruct. 53 (2013) 99–112.
[30] O. Aytekin, S. Turgut, M. Tomak, Nonlinear optical properties of a Pöschl–Teller quantum well under electric and magnetic fields, Physica E 44 (2012) 1612–1616.
[31] B.O. Alaydin, Effect of high bandgap AlAs quantum barrier on electronic and optical properties of In0.70Ga0.30As/Al0.60In0.40As superlattice under applied electric field for laser and detector applications, Int. J. Mod. Phys. B 35 (2021) 2150027.
[32] H.S. Aydinoglu, M. Sayrac, M.E. Mora-Ramos, F. Ungan, Nonlinear optical properties in AlxGa1-xAs/GaAs double-graded quantum wells: the effect of the structure parameter, static electric, and magnetic field, Solid State Commun. 342 (2022) 114647.
[33] M. Sayrac, A.J. Peter, F. Ungan, Interband transitions and exciton binding energy in a Razavy quantum well: effects of external fields and Razavy potential parameters, Eur. Phys. J. C Part Fields 137 (2022) 840.
[34] L. Zhang, H.-J. Xie, Electric field effect on the second-order nonlinear optical properties of parabolic and semiparabolic quantum wells, Phys. Rev. B 68 (2003) 235315.
[35] A. Keshavarz, M.J. Karimi, Linear and nonlinear intersubband optical absorption in symmetric double semi-parabolic quantum wells, Phys. Lett. A 374 (2010) 2675–2680.
[36] A.Salman Durmuslar, A. Turkoglu, M.E. Mora-Ramos, F. Ungan, The non-resonant intense laser field effects on the binding energies and the nonlinear optical properties of a donor impurity in Rosen–Morse quantum well, Indian J. Phys. (2022).
[37] İ. Karabulut, S. Baskoutas, Linear and nonlinear optical absorption coefficients and refractive index changes in spherical quantum dots: effects of impurities, electric field, size, and optical intensity, J. Appl. Phys. 103 (2008) 073512.
[38] D. Altun, O. Ozturk, B.O. Alaydin, E. Ozturk, Linear and nonlinear optical properties of a superlattice with periodically increased well width under electric and magnetic fields, Micro Nanostructures (2022) 207225.
[39] Y. Yakar, B. Çakır, A. Özmen, Calculation of linear and nonlinear optical absorption coefficients of a spherical quantum dot with parabolic potential, Optics Commun. 283 (2010) 1795–1800.
[40] B.O. Alaydin, D. Altun, E. Ozturk, Linear and nonlinear optical properties of semi-elliptical InAs quantum dots: effects of wetting layer thickness and electric field, Thin. Solid. Films 755 (2022) 139322.
[41] F. Ungan, U. Yesilgul, S. Şakiroğlu, E. Kasapoglu, H. Sari, I. Sökmen, Effects of an intense, high-frequency laser field on the intersubband transitions and impurity binding energy in semiconductor quantum wells, Phys. Lett. A 374 (2010) 2980–2984.
[42] F. Ungan, U. Yesilgul, E. Kasapoglu, H. Sari, I. Sökmen, Effects of applied electromagnetic fields on the linear and nonlinear optical properties in an inverse parabolic quantum well, J. Lumin. 132 (2012) 1627–1631.
[43] F. Ungan, U. Yesilgul, S. Sakiroglu, E. Kasapoglu, H. Sari, I. Sökmen, The effect of hydrostatic pressure on subband structure and optical transitions in modulation-doped quantum well, Superlattices Microstruct. 49 (2011) 635–643.
[44] S. Sakiroglu, U. Yesilgul, F. Ungan, C.A. Duque, E. Kasapoglu, H. Sari, I. Sokmen, Electronic band structure of GaAs/AlxGa1−xAs superlattice in an intense laser field, J. Lumin. 132 (2012) 1584–1588.
[45] N. Eseanu, Simultaneous effects of laser field and hydrostatic pressure on the intersubband transitions in square and parabolic quantum wells, Phys. Lett. A 374 (2010) 1278–1285.
[46] M.E. Mora-Ramos, C.A. Duque, E. Kasapoglu, H. Sari, I. Sökmen, Electron-related nonlinearities in GaAs–Ga1−xAlxAs double quantum wells under the effects of intense laser field and applied electric field, J. Lumin. 135 (2013) 301–311.
[47] G.-H. Wang, Q. Guo, K.-X. Guo, Refractive index changes induced by the incident optical intensity in semiparabolic quantum wells, Chin. J. Phys. 41 (2003) 296–306.
[48] S. Ünlü, İ. Karabulut, H. Şafak, Linear and nonlinear intersubband optical absorption coefficients and refractive index changes in a quantum box with finite confining potential, Physica E 33 (2006) 319–324.
[49] A. Doyeol, C. Shun-lien, Calculation of linear and nonlinear intersubband optical absorptions in a quantum well model with an applied electric field, IEEE J. Quantum Electron. 23 (1987) 2196–2204.
[50] R. Khordad, Effect of position-dependent effective mass on linear and nonlinear optical properties of a cubic quantum dot, Physica B 406 (2011) 3911–3916.
[51] F. Ungan, E. Kasapoglu, C.A. Duque, H. Sari, I. Sokmen, The effect of the intense laser field on the intersubband transitions in Ga1−xInxNyAs1−y/GaAs single quantum well, Physica E 44 (2011) 515–520.
[52] H. Dakhlaoui, F. Ungan, J.C. Martínez-Orozco, M.E. Mora-Ramos, Theoretical investigation of linear and nonlinear optical properties in an heterostructure based on triple parabolic barriers: effects of external fields, Physica B 607 (2021) 412782.
[53] H. Dakhlaoui, M. Nefzi, Tuning the linear and nonlinear optical properties in double and triple $\delta-$ doped GaAs semiconductor: impact of electric and magnetic fields, Superlattices Microstruct. 136 (2019) 106292.
[54] A.Salman Durmuslar, H. Dakhlaoui, M.E. Mora-Ramos, F. Ungan, Effects of external fields on the nonlinear optical properties of an n-type quadruple δ-doped GaAs quantum wells, Eur. Phys. J. C Part Fields 137 (2022) 730.
[55] M. Sayrac, J.C. Martínez-Orozco, M.E. Mora-Ramos, F. Ungan, The nonlinear optical rectification, second and third harmonic generation coefficients of Konwent potential quantum wells, Eur. Phys. J. C Part Fields 137 (2022) 1033.
[56] O. Ozturk, E. Ozturk, S. Elagoz, Linear and nonlinear optical absorption coefficient and electronic features of triple GaAlAs/GaAs and GaInAs/GaAs quantum wells depending on barrier widths, Optik 180 (2019) 394–405.

Journal of Molecular Structure

| Supports *open access*

Articles & Issues | About | Publish | Order journal | Search in this journal

Abstracting and indexing

- Chemical Abstracts
- Current Contents - Physical, Chemical & Earth Sciences
- Mass Spectrometry Bulletin
- Pascal Francis
- Science Citation Index
- Science Citation Index Expanded
- Scopus
- INSPEC

View historical data and other metrics

Journal Insights

Aims & scope

The *Journal of Molecular Structure* is dedicated to the publication of full-length articles and review papers, providing important **new structural information** on all types of chemical species including:

• Stable and unstable **molecules** in all types of environments (vapour, molecular beam, liquid, ...

View full aims & scope

ISSN

Online ISSN: 1872-8014 | Print ISSN: 0022-2860

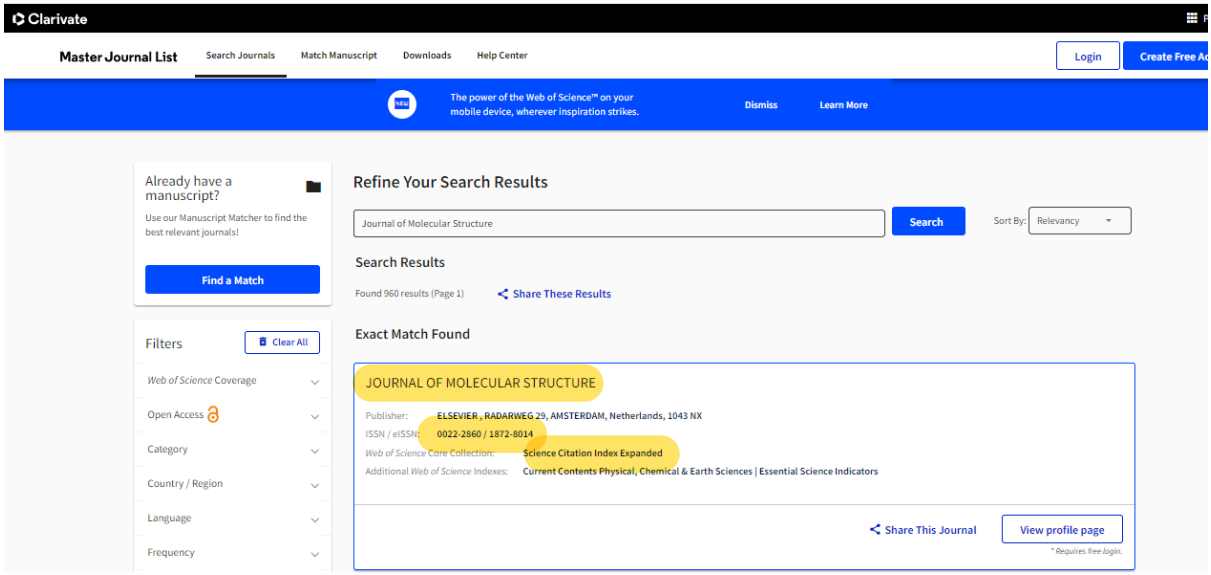

JOURNAL OF MOLECULAR STRUCTURE

Publisher name: ELSEVIER

Journal Impact Factor ™

3.8	3.2
2022	Five Year

JCR Category	Category Rank	Category Quartile
CHEMISTRY, PHYSICAL *in SCIE edition*	74/161	Q2

Source: Journal Citation Reports 2022. Learn more

Journal Citation Indicator ™ New

0.57	0.52
2022	2021

JCI Category	Category Rank	Category Quartile
CHEMISTRY, PHYSICAL *in SCIE edition*	89/172	Q3